



## Experimental, quantum chemical and Monte Carlo simulations studies on the corrosion inhibition of mild steel in 1 M HCl by two benzothiazine derivatives

M. Saadouni<sup>1</sup>, M. Galai<sup>2</sup>, Y. El Aoufir<sup>3,4\*</sup>, S. Skal<sup>4</sup>, S. Boukhris<sup>1</sup>, A. Hassikou<sup>1</sup>,  
M. Ebn Touhami<sup>2</sup>, A. Guenbour<sup>4</sup>, A. El khlifi<sup>5</sup>, H. Oudda<sup>3</sup>, N. Habbadi<sup>1</sup>, A. Souizi<sup>1</sup>

1. Laboratory of Organic, Organometallic and Theoretical Chemistry, Faculty of Science,  
Ibn Tofail University, 14000 Kenitra, Morocco

2. Laboratory of Materials Engineering and Environment: Modeling and Applications (LMEEMA), Faculty of Sciences,  
University Ibn Tofail, BP 133, 14 000 Kenitra, Morocco

3. Laboratory separation processes, Faculty of Science, University Ibn Tofail PO Box 242, Kenitra, Morocco.

4. Laboratory of Nanotechnology, Materials & Environment, Faculty of Sciences, Mohammed V University, Rabat,  
Morocco

5. Laboratoire de Biotechnologie, Environnement et Qualité, Faculté des Sciences, Université Ibn Tofail, 14000 Kénitra

Received 02 Aug 2017,

Revised 26 May 2018,

Accepted 28 May 2018

### Keywords

- ✓ Benzothiazine;
- ✓ Corrosion inhibition;
- ✓ Mildsteel;
- ✓ MonteCarlo;
- ✓ HCl
- ✓ Electrochemicalmethods

Y. El Aoufir :  
[eyasmina1@gmail.com](mailto:eyasmina1@gmail.com)

### Abstract

Two benzothiazine derivatives namely, Methyl 3-hydroxy-2-(p-tolyl)-3,4-dihydro-2H-benzo[b][1,4]thiazine-3-carboxylate (MBT), Ethyl 3-hydroxy-2-(p-tolyl)-3,4-dihydro-2H-benzo[b][1,4]thiazine-3-carboxylate (EBT) were examined as a corrosion inhibitors for mild steel in 1.0 M HCl using electrochemical impedance spectroscopy (EIS) and potentiometric polarization (PDP). The results show that both compounds are good inhibitors and their inhibition efficiencies reached 97% at  $10^{-3}$  M. The percentage inhibition efficiency ( $\eta$  %) increased with the increase of inhibitor concentration due to the adsorption of the inhibitory molecules on the metal surface. The Tafel polarization study revealed that both inhibitors act as a mixed type inhibitor. Furthermore, it has been established that the adsorption follows the Langmuir adsorption isotherm. Quantum chemical parameters were calculated using the Density Functional Theory (DFT) method and Monte Carlo simulations. The correlation between theoretical and experimental results was discussed.

## 1. Introduction

The mild steel is one of the most metals used in industry, but, the use of the acid solutions in some industrial processes such as drilling operations in oil, gas exploration, pickling, and acid cleaning of steel structures, resulting a considerable corrosion of the metal[1].

The inhibitors are widely used in order to protect the metallic materials against degradation due to corrosion [2–5]. Organic compounds have become most accepted as effective corrosion inhibitors in various media in order to inhibit the corrosion reaction and reduce the corrosion rate by blocking the metal from coming into contact with the corrosive solution.

A continuing effort has been made to develop a corrosion inhibitor that exhibits a greater inhibition effect at a low concentration in the corrosion medium as well as environment-friendly feature[1,4,6]. Most of the acid corrosion inhibitors are organic compounds containing electronegative atoms (such as O, N, S, and P etc.), unsaturated bonds and/or aromatic rings. The inhibitory performance of organic compounds is due to the adsorptive layer forming between the molecules with lone electron pair and/or  $\pi$  electrons and the surface metal atoms with unoccupied d-orbitals[2,5,7–10]. Meanwhile, the use of quantum chemical calculations has been proved to be a useful tool in elucidating the mechanism of inhibition of corrosion inhibitors on metal surface at the molecular level; and, it can provide theoretical support in searching for new inhibitors[11–13].

Interestingly, there is a great interest in 1,4-benzothiazines and are increasingly being investigated for applications in the growing field of medicine. In fact, the 1,4-benzothiazines are the best known to possess biologically diverse activities [14] such as antimicrobial [15] antifungal [16] antioxidant agents [17] and

anticancer [18,19]. In previous work, the corrosion inhibition of benzothiazine derivatives was examined by electrochemical measurements (1,2,3). The authors suggest that the inhibition efficiency is linked to the concentration and molecular structure of the molecules [20].

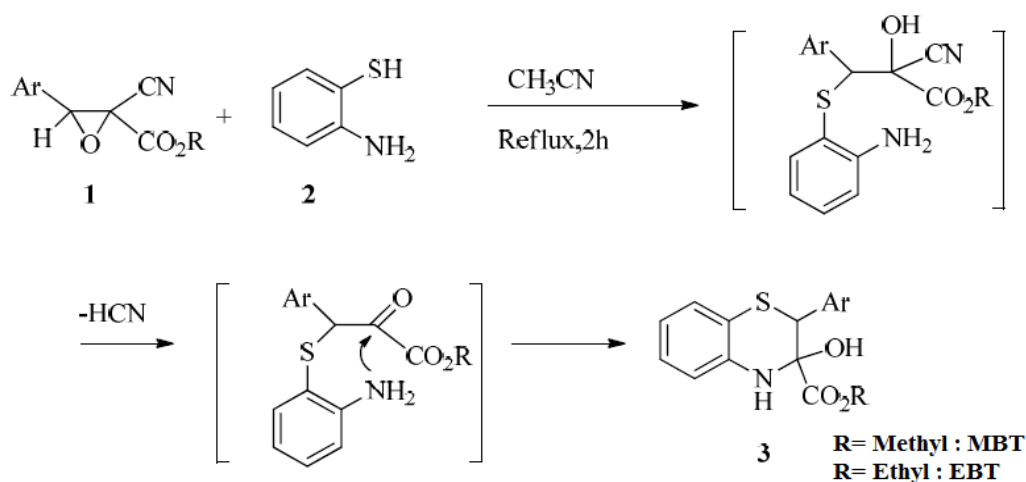
Density functional theory (DFT) for instance, has been used to predict the molecular geometry, electronic properties and active sites of organic corrosion inhibitors[21]. This could help in the understanding of specific sites of interaction between the inhibitor and the metal surface. On the other hand, Monte Carlo simulation can provide us useful information about the low energy adsorption configuration of an organic inhibitor onto a metal surface which cannot be evaluated experimentally [22].

In this paper, electrochemical techniques were employed to study the inhibition effect of two 1,4-benzothiazines for mild steel in 1.0 M HCl solution. And then, quantum chemical calculations by Monte Carlo simulation and DFT method at B3LYB basis set, were performed to obtain more information about the interaction between the inhibitor molecules and mild steel surface.

## 2. Materials and methods

### 2.1. Synthesis

*General procedure for the preparation of two 1,4-benzothiazines derivatives:* To a solution of epoxide **1** (1 mmol) in acetonitrile (20 mL), are added the 2-aminothiophenol (1 mmol). The mixture is refluxed for 25 h. The hydrogen cyanide is trapped by a solution 0.1N KOH in a bubbler. Then, the solvent is removed under reduced pressure and the residue obtained is purified by flash chromatography on silica column eluted with chloroform / petroleum ether 2:1.

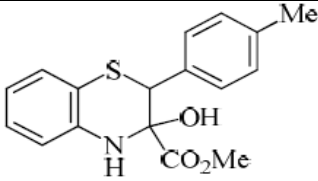
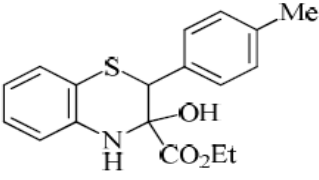


**Figure 1.** Synthesis of 1,4-benzothiazines derivatives.

**Methyl 3-hydroxy-2-(p-tolyl)-3,4-dihydro-2H-benzo[b][1,4]thiazine-3-carboxylate(MBT):** 0.18 g (60%); M.p. 188-190 °C; IR (KBr) cm<sup>-1</sup>: 3483 (NH), 2983 (OH), 1742 (CO). The signals of diastereomer1 : <sup>1</sup>H NMR (300 MHz, DMSO-d<sub>6</sub>):  $\delta$  2.31 (s, 3H, CH<sub>3</sub>), 4.74 (s, 1H, CHS), 3.82 (s, 3H, CO<sub>2</sub>Me), 5.41 (s, 1H, OH); 6.38-7.35 (m, Ar); <sup>13</sup>C NMR (75 MHz, DMSO-d<sub>6</sub>):  $\delta$  21.34, 54.55, 64.31, 83.0, 114.33, 115.27, 116.92, 127.18, 127.96, 129.58, 131.62, 135.86, 140.19, 150.15, 163.31. The signals of diastereomer2 : <sup>1</sup>H NMR (300 MHz, DMSO-d<sub>6</sub>):  $\delta$  2.48 (s, 3H, CH<sub>3</sub>), 4.74 (s, 1H, CHS), 3.82 (s, 3H, CO<sub>2</sub>Me), 5.41 (s, 1H, OH); 6.38-7.35 (m, Ar); <sup>13</sup>C NMR (75 MHz, DMSO-d<sub>6</sub>):  $\delta$  21.34, 54.0, 64.31, 83.0, 114.33, 115.27, 116.92, 127.18, 127.96, 129.58, 131.62, 135.86, 140.19, 150.15, 166.0.; EIMS: m/z (C<sub>17</sub>H<sub>17</sub>NO<sub>3</sub>S) 315 (M<sup>+</sup>, 46.6%), 297(M<sup>+</sup>-H<sub>2</sub>O, 52.7%), 225 (100%), 135 (31.5 %), 119 (28.4%).

**Ethyl 3-hydroxy-2-(p-tolyl)-3,4-dihydro-2H-benzo[b][1,4]thiazine-3-carboxylate(EBT):** 0.19 g (60%); IR (KBr) cm<sup>-1</sup>: 3378 (NH), 2982 (OH), 1746 (CO). The signals of diastereomer 1: <sup>1</sup>H NMR (300 MHz, DMSO-d<sub>6</sub>):  $\delta$  2.40 (s, 3H, CH<sub>3</sub>), 4.7 (s, 1H, CHS), 1.28 (t, 3H, CO<sub>2</sub>CH<sub>2</sub>CH<sub>3</sub>), 4.7(q, 2H, CO<sub>2</sub>CH<sub>2</sub>CH<sub>3</sub>), 6.4-7.5 (m, Ar); <sup>13</sup>C NMR (75 MHz, DMSO-d<sub>6</sub>):  $\delta$  14.21, 21.49, 57.0, 63.92, 83.92, 115.28, 116.56, 122.69, 125.80, 127.22, 128.01, 130.36, 134.81, 140.14, 150.21, 162.77. The signals of diastereomer 2: <sup>1</sup>H NMR (300 MHz, DMSO-d<sub>6</sub>):  $\delta$  2.30 (s, 3H, CH<sub>3</sub>), 4.7 (s, 1H, CHS), 1.21 (t, 3H, CO<sub>2</sub>CH<sub>2</sub>CH<sub>3</sub>), 4.29 (q, 2H, CO<sub>2</sub>CH<sub>2</sub>CH<sub>3</sub>), 6.4-7.5 (m, Ar); <sup>13</sup>C NMR (75 MHz, DMSO-d<sub>6</sub>):  $\delta$  14.31, 21.34, 57.0, 62.37, 83.92, 114.29, 117.01, 123.17, 127.01, 127.59, 129.55, 130.75, 135.90, 141.92, 154.08, 167.0.; EIMS: m/z (C<sub>18</sub>H<sub>19</sub>NO<sub>3</sub>S) 225 (100%), 116 (7.14%), 91 (7.14%), 108(17.14%).

**Table 1.** Molecular structures and abbreviation of tested inhibitors.

Compound	Names and abbreviation
	Methyl 3-hydroxy-2-(p-tolyl)-3,4-dihydro-2H-benzo[b][1,4]thiazine-3-carboxylate [MBT]
	Ethyl 3-hydroxy-2-(p-tolyl)-3,4-dihydro-2H-benzo[b][1,4]thiazine-3-carboxylate [EBT]

## 2.2. Materials

The steel used in this study is a carbon steel (CS) (Euronorm: C35E carbon steel and US specification: SAE 1035) with a chemical composition (in wt%) of 0.370 % C, 0.230 % Si, 0.680 % Mn, 0.016 % S, 0.077 % Cr, 0.011 % Ti, 0.059 % Ni, 0.009 % Co, 0.160 % Cu and then remainder iron (Fe). The aggressive solution of 1.0 M HCl was prepared by dilution of analytical grade 37% HCl with distilled water. The concentration range of the investigated compound was  $10^{-6}$  to  $5 \times 10^{-3}$  M.

## 2.3. Corrosion tests

### 2.3.1. Electrochemical impedance spectroscopy

The electrochemical measurements were carried out using Volta lab (Tacussel- Radiometer PGZ 100) potentiostat and controlled by Tacussel corrosion analysis software model (Voltmaster 4) at under static condition. The corrosion cell used had three electrodes. The reference electrode was a saturated calomel electrode (SCE). A platinum electrode was used as auxiliary electrode of surface area of  $1 \text{ cm}^2$ . The working electrode was carbon steel. All potentials given in this study were referred to this reference electrode. The working electrode was immersed in test solution for 30 minutes to establish steady state open circuit potential ( $E_{\text{ocp}}$ ). After measuring the  $E_{\text{ocp}}$ , the electrochemical measurements were performed. All electrochemical tests have been performed in aerated solutions at 303 K to reach the appropriate conditions of corrosion. The EIS experiments were conducted in the frequency range with high limit of 100 kHz and different low limit 0.1 Hz at open circuit potential, with 10 points per decade, at the rest potential, after 30 min of acid immersion, by applying 10 mV ac voltage peak-to-peak. Nyquist plots were made from these experiments. The best semicircle can be fit through the data points in the Nyquist plot using a non-linear least square fit so as to give the intersections with the x-axis.

The inhibition efficiency of the inhibitor was calculated from the charge transfer resistance values using the following equation:

$$\eta_{\text{EIS}} \% = \frac{R_p^{\circ} - R_p^i}{R_p^i} \times 100 \quad (1)$$

where,  $R_p^{\circ}$  and  $R_p^i$  are the polarization resistance in absence and in presence of inhibitor, respectively.

### 2.3.2. Potentiodynamic polarization

The electrochemical behaviour of carbon steel sample in inhibited and uninhibited solution was studied by recording anodic and cathodic potentiodynamic polarization curves. Measurements were performed in the 1.0 M HCl solution containing different concentrations of the tested inhibitor by changing the electrode potential automatically from -800 mV/SCE to -200 mV/SCE at a scan rate of  $1 \text{ mV s}^{-1}$ . The linear Tafel segments of anodic and cathodic curves were extrapolated to corrosion potential to obtain corrosion current densities ( $i_{\text{corr}}$ ). From the polarization curves obtained, the corrosion current ( $i_{\text{corr}}$ ) was calculated by curve fitting using the equation:

$$i = i_{\text{corr}} \left[ \exp\left(\frac{2.3\Delta E}{\beta_a}\right) - \exp\left(\frac{2.3\Delta E}{\beta_c}\right) \right] \quad (2)$$

$\beta_a$  and  $\beta_c$  are the anodic and cathodic Tafel slopes and  $\Delta E$  is  $E - E_{\text{corr}}$ .

The inhibition efficiency was evaluated from the measured  $i_{\text{corr}}$  values using the relationship:

$$\eta_{\text{PDP}} \% = \frac{i_{\text{corr}}^{\circ} - i_{\text{corr}}^i}{i_{\text{corr}}^{\circ}} \times 100 \quad (3)$$

where  $i_{\text{corr}}^{\circ}$  and  $i_{\text{corr}}^i$  are the corrosion current density in absence and presence of inhibitor, respectively.

#### 2.4. DFT calculations

$E_{\text{HOMO}}$  (highest occupied molecular orbital energy),  $E_{\text{LUMO}}$  (lowest unoccupied molecular orbital energy) and Fukui indices calculations were performed using *DMol<sup>3</sup>* module in Materials Studio version 6.0[23]. These calculations employed an *ab initio*, gradient-corrected functional (*GGA*) method with a double numeric plus polarization (DNP) basis set and a Becke One Parameter (BOP) functional. It is well-known that the phenomena of electrochemical corrosion appear in aqueous phase. *DMol<sup>3</sup>* includes certain COSMO controls, which allow for the treatment of solvation effects[27,28].

#### 2.5. Monte Carlo simulation

Experimentally, a molecular system is described by a small number of parameters, such as volume and temperature. The collection of molecular configurations that satisfy this partial knowledge is called an ensemble of configurations. Adsorption Locator module as implemented in the Materials Studio 6.0 software (Accelrys, Inc.) has been employed to compute the interaction between tested benzodiazepine derivatives and Fe (110) surface through Metropolis Monte Carlo approach[23]. A simulation box ( $29.78 \times 29.78 \times 60.13 \text{ \AA}$ ) has been constructed to simulate the interaction between tested inhibitors and the Fe (110) surface. COMPASS force field was used to optimize the structures of all components of the system of interest.

### 3. Results and Discussions

#### 3.1. Effect of concentration

##### 3.1.1. Tafel Polarization Study

The potentiodynamic polarization measurements were carried out to study the kinetics of the cathodic and anodic reactions. Fig. 2 shows the results of the effect of MBT and EBT on the cathodic as well as anodic polarization curves of mild steel in 1 M HCl. It is evident from the figure that both reactions were suppressed with the addition of the inhibitor. This suggests that the two reduced the anodic dissolution reactions as well as retarded the hydrogen evolution reactions on the cathodic sites.

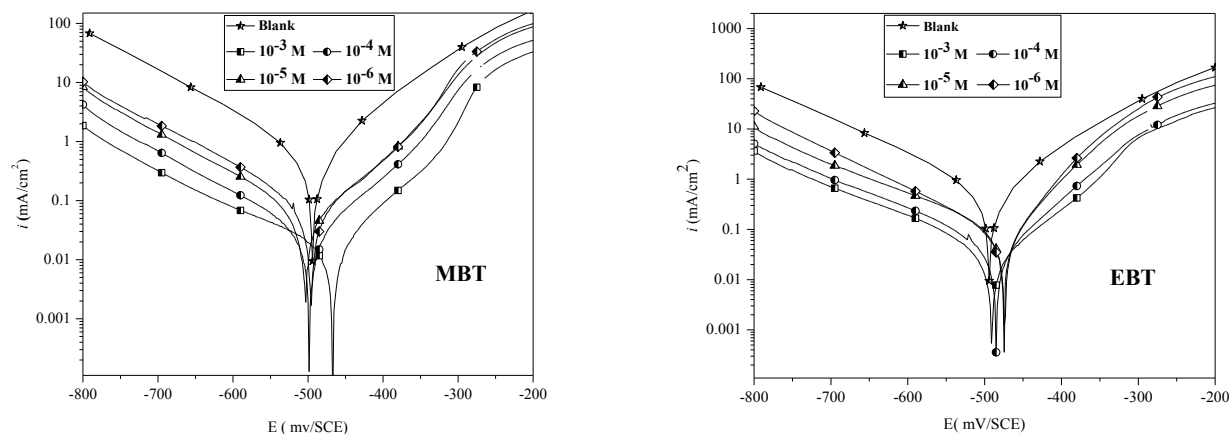


**Figure 2.** Polarization curves of mild steel in 1.0 M HCl without and with different concentrations of inhibitors at 303 K.

Electrochemical corrosion kinetic parameters namely corrosion potential ( $E_{\text{corr}}$ ) and corrosion current density ( $i_{\text{corr}}$ ) obtained from the extrapolation of the cathodic polarization curves are listed in Table 2. The corrosion current density ( $i_{\text{corr}}$ ) decreased by the increase in the adsorption of the inhibitors with increasing inhibitor concentration. The inhibition efficiency increases with increase in the inhibitor concentration was calculated by the  $i_{\text{corr}}$  values and listed in Table 2. If the displacement in corrosion potential is more than 85 mV with respect

to the corrosion potential of blank solution, the inhibitor can be consider as a cathodic or anodic type[26,27]. In present study, displacement was 85 mV with respect to the corrosion potential of the uninhibited sample which indicates that the studied inhibitors is a mixed type of inhibitors.

Also, the Tafel plots indicate that the mechanism of hydrogen reduction is activation control. The presence of tested inhibitors does not affect the cathodic Tafel slope, indicating that the mechanism of H<sup>+</sup> reduction is not modified with the **MBT** and **EBT** concentration. Also, the corrosion potential is almost constant in the presence of the inhibitors. The inhibitor molecules decrease the surface area of corrosion and only cause inactivation of a part of the surface with respect to the corrosion medium. This phenomenon is interpreted by the adsorption of the molecules on steel surface leading to the increase of the surface coverage. On the other hand, the desorption process of the molecules from the surface was observed with MBT more than the EBT, which the desorption potential increases with increasing the concentration.

**Table 2.** Electrochemical parameters and corresponding inhibition efficiency for corrosion of the mild steel in 1.0 M HCl in the absence and the presence of different concentrations of inhibitors at 303 K.

Inhibitor	Concentration (M)	$-E_{\text{corr}}$ (mV/SCE)	$-\beta_c$ (mV/dec)	$\beta_a$ (mV/dec)	$i_{\text{corr}}$ ( $\mu\text{A}/\text{cm}^2$ )	$\eta_{\text{PDP}}$ (%)
Blank	1.0	496	162	132.2	564	-
<b>MBT</b>	$1 \times 10^{-3}$	471	160	101	17	97
	$1 \times 10^{-4}$	505	159	114	28	95
	$1 \times 10^{-5}$	506	156	115	71	87
	$1 \times 10^{-6}$	500	153	119	90	84
<b>EBT</b>	$1 \times 10^{-3}$	494	154	98	53	90
	$1 \times 10^{-4}$	486	157	99	65	88
	$1 \times 10^{-5}$	475	150	101	87	84
	$1 \times 10^{-6}$	478	155	107	107	81

### 3.1.2. Electrochemical impedance spectroscopy (EIS)

The inhibition performance of MBT and EBT for the acid corrosion of mild steel was evaluated by EIS. Fig. 3 shows the Nyquist plots in 1.0 M hydrochloric acid solution containing different concentrations of both inhibitors.

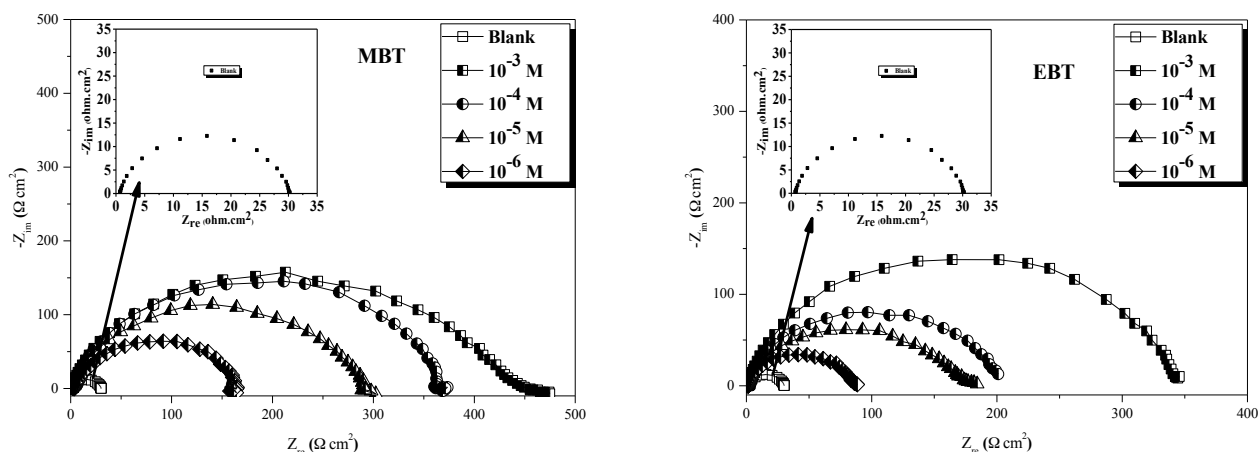


**Figure 3.** Nyquist plots of mild steel in 1.0M HCl at different concentrations of inhibitors at 303K.

The irregular semicircles derived from impedance data indicate a non-ideal electrochemical behavior on the electrode surface, which may be due to frequency dispersion, inhomogeneties, roughness of metal surface and substance transmission actions[28,29]. As can be seen from Fig. 3, the Nyquist diagrams in the presence of

inhibitors are similar to the blank one, this remark suggest that the inhibitor compounds block the corrosion behavior of mild steel by controlling the activation of electrochemical reaction without changing its nature. In Fig. 3 we can only observe a capacitive loop which is related to the behavior of double layer capacitance as well as the charge transfer process between metal surface and electrolyte[30,31]. The diameters of Nyquist plots increase as the concentration of inhibitor rises, suggesting the enhanced protection effect of inhibitor on the damage of metal in the corrosive solution[32].The impedance spectra were fitted to the  $R_s(R_{ct}/CPE)$  equivalent circuit of the form in Fig. 4.

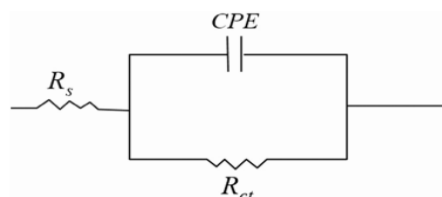


**Figure 4.**Equivalent electrical circuit.

where  $R_s$  is the solution resistance,  $R_{ct}$  denotes the charge-transfer resistance and  $CPE$  is constant phase element. The introduction of  $CPE$  into the circuit was necessitated to explain the depression of the capacitance semicircle, which corresponds to surface heterogeneity resulting from surface roughness, impurities, and adsorption of inhibitors[33–35]. The impedance of this element is frequency-dependent and can be calculated using the Eq. 4:

$$Z_{CPE} = \frac{1}{Q(j\omega)^n} \quad (4)$$

where,  $Q$  is the  $CPE$  constant (in  $\Omega^{-1} S^n cm^{-2}$ ),  $\omega$  is the angular frequency (in  $rad s^{-1}$ ),  $j^2 = -1$  is the imaginary number and  $n$  is a  $CPE$  exponent which can be used as a gauge for the heterogeneity or roughness of the surface[36,37]. In addition, the double layer capacitances,  $C_{dl}$ , for a circuit including a  $CPE$  were calculated by using the following Eq. 5:

$$C_{dl} = \sqrt[n]{Q \times R_{ct}^{1-n}} \quad (5)$$

The values of EIS parameters namely, polarization resistance ( $R_p$ ), double layer capacitance ( $C_{dl}$ ), phase shift ( $n$ ), and inhibition efficiency ( $\eta_{EIS}$  %) were calculated with the help of equivalent circuit (shown in Fig. 4) and are reported in Table 3.

**Table 3.** Impedance parameters recorded for carbon steel electrode in 1 M HCl solution in the absence and presence of different concentrations of inhibitors at 303K.

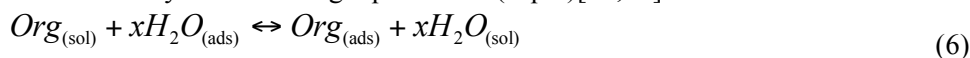
Inhibitor	Concentration (M)	$R_{ct}$ ( $\Omega \times cm^2$ )	$n$	$Q \times 10^{-4}$ ( $s^n / \Omega \times cm^2$ )	$C_{dl}$ ( $\mu F/cm^2$ )	$\eta_{EIS}$ (%)
<b>Blank</b>	1.0	29.35	0.89	1.7610	91	-
<b>MBT</b>	$1 \times 10^{-3}$	414	0.81	0.3034	10	97
	$1 \times 10^{-4}$	361	0.83	0.3456	14	96
	$1 \times 10^{-5}$	274	0.85	0.3987	18	94
	$1 \times 10^{-6}$	59	0.86	0.7667	31	76
<b>EBT</b>	$1 \times 10^{-3}$	336	0.86	0.4556	23	96
	$1 \times 10^{-4}$	213	0.88	0.4766	25	93
	$1 \times 10^{-5}$	168	0.84	0.6877	29	91
	$1 \times 10^{-6}$	56	0.87	0.7888	35	75

It can be seen from the results that the values of  $R_{ct}$  significantly increase whereas the values of  $C_{dl}$  decrease in the presence of both compounds. This increase in  $R_p$  and decrease in  $C_{dl}$  values in the presence of studied inhibitors is attributed to a decrease in local dielectric constant and/or to an increase in the thickness of the electrical double layer[38]. These results suggest the formation of protective inhibitor film by adsorbing at the metal/electrolyte interfaces. The values of inhibition efficiency ( $\eta_{EIS}$ %) increase with the concentration of

inhibitors up to 97% and 96% for P-1 and P-2 respectively. These results confirm once again that the studied compounds exhibit efficient inhibitive performance for mild steel in hydrochloric acid solution.

### 3.2. Adsorption isotherm

Adsorption study was performed to understand the inhibiting effect of organic molecules on metal corrosion. It is accepted that inhibitor covers the iron surface by replacing the pre-adsorbed water molecules which act as a corrosive medium by the following equilibrium (Eq. 6)[39,40].



where  $Org_{(sol)}$  and  $Org_{(ads)}$  are the organic molecules in the aqueous solution and adsorbed on the metallic surface, respectively,  $H_2O_{(ads)}$  is the water molecules on the metallic surface, and  $n$  is the number of water molecules replaced by the organic molecules [41]. When the equilibrium of the process described in this equation is reached, it is possible to obtain different expressions of the adsorption isotherm plots, and thus the surface coverage degree ( $\theta$ ) can be plotted as a function of the concentration of the inhibitor under test[42].

At present, adsorption isotherm can provide meaningful information about the interaction between additive and mild steel, based on the inference that the coverage of organic molecules is directly related to inhibition efficiency.

The degree of surface coverage ( $\theta$ ) was used to evaluate the best isotherm that fits into the data obtained. Langmuir isotherm was applied to investigate whether it best fits to the experimental data obtained by using Eq. (7)[43–45].

$$\frac{C_{inh}}{\theta} = \frac{1}{K_{ads}} + C_{inh} \quad (7)$$

where  $C_{inh}$  is the inhibitor concentration,  $K_{ads}$  is the equilibrium constant for the adsorption–desorption process and  $\theta$  is the surface coverage. The values of  $K_{ads}$  were calculated with the help of the Langmuir plot shown in Fig. 5. The  $K_{ads}$  is related to the standard free energy ( $\Delta G_{ads}^\circ$ ) of adsorption by the relation[46].

$$\Delta G_{ads}^\circ = -RT \ln(K_{ads} \times 55.5) \quad (8)$$

where  $R$  is the universal gas constant,  $T$  is the absolute temperature in K, and the numerical value 55.5 represents the molar concentration of water in the acid solution. The calculated values of  $K_{ads}$  and  $\Delta G_{ads}^\circ$  at 303K are listed in Table 4.

Generally, a value of  $\Delta G_{ads}^\circ$  of  $-20 \text{ kJ mol}^{-1}$  or less negative is associated with physical adsorption resulting from electrostatic interaction between a charged inhibitor and charged metal, and a value of  $\Delta G_{ads}^\circ$  of  $-40 \text{ kJ mol}^{-1}$  or more negative is associated with chemical adsorption resulting from charged (electron) sharing between non-bonding electrons of the inhibitor and the d-orbital's of the surface Fe-atoms [47,48]. In our present study, the values of  $\Delta G_{ads}^\circ$  were found to be between  $-48$  and  $-44 \text{ kJ mol}^{-1}$ , suggesting that the investigated benzothiazine derivatives are adsorbed on the mild steel surface by a chemisorption mechanism.

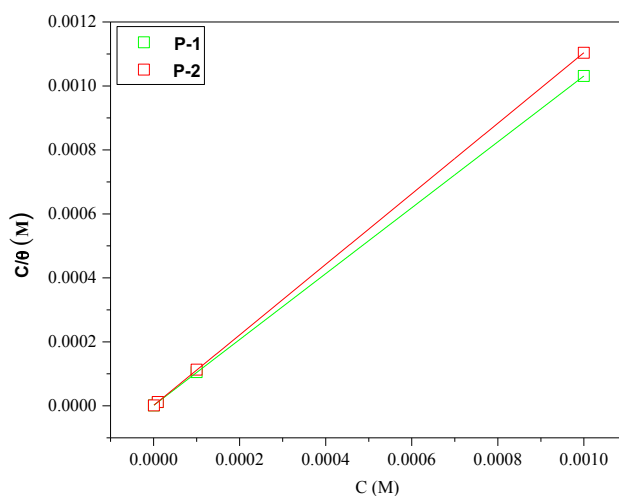


**Figure 5.** Langmuir adsorption isotherm plots for both inhibitors at 303K.

**Table 4.** Adsorption parameters of studied inhibitors for mild steel corrosion in 1.0 M HCl at 303 K.

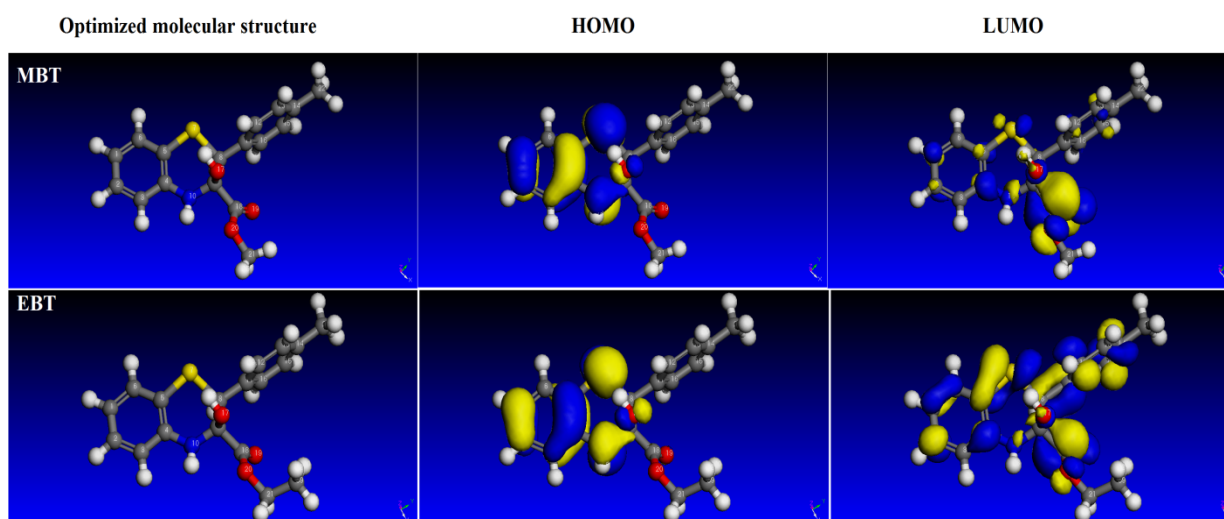
Inhibitor	Slope	$K_{ads}(M^{-1})$	$R^2$	$\Delta G_{ads}^{\circ}$ (kJ/mol)
MBT	1.01	879437	0.9999	-48.84
EBT	1.04	849386	0.9999	-44.48

### 3.3. Quantum chemical calculations

DFT based quantum chemical (QC) calculations were performed on MBT and EBT to find more insight about the chemical reactivity of these compounds. The optimized and frontier molecular electron distribution pictures of MBT and EBT are shown in Figs. 6. From Fig. 6, it could be seen that both inhibitors have similar HOMO and LUMO distributions, which were all located on the benzothiazine segment. This is due to the presence of heteroatoms together with several  $\pi$ -electrons on the molecular structure of both inhibitors. Some common QC indices such as  $E_{HOMO}$  (energy of highest molecular orbital),  $E_{LUMO}$  (lowest unoccupied molecular orbital),  $\Delta E$  (energy band gap), and fraction of electron transfer ( $\Delta N$ ). The quantum chemical calculation parameters are derived from MBT and EBT are listed in Table 5. It can be seen from the results depicted in Table 5 that values of different quantum chemical calculation parameters derived for MBT and EBT show a regular trend. In general, a higher value of  $E_{HOMO}$ , is associated with high electron donating ability while, lower value of  $E_{LUMO}$  is associated with strong interactions between the inhibitor and a metallic surface and therefore a higher value of  $E_{HOMO}$  and/ or a lower value of  $E_{LUMO}$  is consistent with high electron donating ability and thereby high inhibition efficiency[49–53]. In the present study values of  $E_{HOMO}$  and  $E_{LUMO}$  for MBT and EBT show regular trend. However, the value of energy band gap ( $\Delta E$ ) is less lower for MBT (3.45 eV) as compared to the EBT (3.47 eV), which indicates that MBT is relatively more reactive chemical species and therefore acts as better corrosion inhibitor as compared to the EBT[50,54].

**Table 5.** Quantum theoretical parameters for both inhibitors.

Inhibitor	$E_{HOMO}$	$E_{LUMO}$	$\Delta E$	$\Delta N$
MBT	-4.022	-0.569	3.45	0.730
EBT	-4.027	-0.554	3.47	0.728

**Figure 6.** Optimized structure and frontier molecular orbital density distributions of studied inhibitors.

According to Koopman's theorem [55] the ionization potential (I) and electron affinity (A) of the inhibitors are calculated using the following equations.

$$I = -E_{HOMO} \quad (9)$$

$$A = -E_{LUMO} \quad (10)$$

Thus, the values of the electronegativity ( $\chi$ ) and the chemical hardness ( $\eta$ ) according to Pearson, operational and approximate definitions can be evaluated using the following relations[56]:

$$\chi = \frac{I+A}{2} \quad (11)$$

$$\eta = \frac{I-A}{2} \quad (12)$$

The number of transferred electrons ( $\Delta N$ ) was also calculated depending on the quantum chemical method[57–59] by using the equation:

$$\Delta N = \frac{\phi - \chi_{inh}}{2(\eta_{Fe} + \eta_{inh})} \quad (13)$$

The obtained DFT derived  $\phi$  values for Fe (1 0 0), Fe (1 1 0) and Fe (1 1 1) surfaces are 3.91, 4.82 and 3.88 eV, respectively[60,61]. In this study, we use only Fe (1 1 0) surface due to its higher stabilization energy and packed surface.

The fraction of electrons transferred  $\Delta N$  from inhibitor to carbon steel surface is also calculated. It has reported that the  $\Delta N$  value measures the ability of a chemical compound to transfer its electrons to metal if  $\Delta N > 0$  and vice versa if  $\Delta N < 0$  [62,63]. In this study, the positive value of  $\Delta N$  presented in Table 5, suggest the high capability of both compounds to donate electrons to the carbon steel surface.

Fukui functions are used to measure the local reactivity of the inhibitors molecules and indicate their chemical reactivity for nucleophilic and electrophilic nature[64,65]. Using a scheme of finite difference approximations, this procedure condenses the values around each atomic site into a single value that characterizes the atom in the molecule. With this approximation, the condensed Fukui function becomes[66]:

$$f_k^+ = q_k(N + 1) - q_k(N) \quad (\text{For nucleophilic attack}) \quad (14)$$

$$f_k^- = q_k(N) - q_k(N - 1) \quad (\text{For electrophilic attack}) \quad (15)$$

Where  $q_k(N+1)$ ,  $q_k(N)$ ,  $q_k(N-1)$  represent charge values of atom  $k$  for anion, neutral, and cation, respectively. The preferred site for nucleophilic attack is the atom in the molecule where the value of  $f^+$  is the highest while the preferred site for electrophilic attack is the atom in the molecule where the value of  $f^-$  is the highest[67]. The values of calculated Fukui functions based on Mulliken population analysis, given in Table 6.

**Table 6.** Values of the Fukui functions for both inhibitors.

Atom	MBT		EBT		
	$f^+$	$f^-$	$f^+$	$f^-$	
C (1)	0.023	0.042	C (1)	0.009	0.053
C (2)	0.027	0.030	C (2)	0.035	0.030
C (3)	0.006	0.023	C (3)	0.019	0.015
C (4)	0.015	0.029	C (4)	0.011	0.033
C (5)	0.011	0.014	C (5)	0.018	0.016
C (6)	0.005	0.017	C (6)	0.017	0.009
S (7)	<b>0.091</b>	<b>0.194</b>	S (7)	<b>0.095</b>	<b>0.180</b>
C (8)	-0.007	-0.016	C (8)	-0.007	-0.011
C (9)	-0.002	-0.020	C (9)	-0.004	-0.022
N (10)	-0.008	<b>0.078</b>	N (10)	0.006	<b>0.078</b>
C (11)	-0.026	-0.015	C (11)	0.011	-0.033
C (12)	0.021	-0.009	C (12)	0.038	-0.003
C (13)	0.011	0.010	C (13)	0.018	0.000
C (14)	0.010	0.009	C (14)	0.007	0.022
C (15)	0.028	0.009	C (15)	0.055	-0.006
C (16)	-0.004	-0.000	C (16)	-0.007	0.006
O (17)	0.018	<b>0.049</b>	O (17)	0.011	<b>0.061</b>
C (18)	<b>0.130</b>	0.006	C (18)	<b>0.062</b>	0.005
O (19)	<b>0.113</b>	0.038	O (19)	<b>0.062</b>	0.031
O (20)	0.045	-0.000	O (20)	0.008	0.020
C (21)	-0.028	-0.011	C (21)	-0.005	-0.025
C (22)	-0.010	-0.008	C (22)	-0.010	-0.011
			C (39)	-0.017	0.001

In MBT and EBT, atoms S7, C18, and O19 present the highest values of  $f_k^+$ , where are the most susceptible sites for nucleophilic attacks. On the other hand S7, N10, and O17 atoms are the susceptible sites for electrophilic attacks as they present the highest values of  $f_k^-$ . The information obtained from the Fukui condensed function entirely agrees with the analysis of the FMO.

### 3.4. Monte Carlo simulation

Monte Carlo simulations were carried out to better understand the interaction between the both inhibitors and Fe (110) surface because it provides some essential parameters such as adsorption energy. In our present study the Monte Carlo simulation calculation was used to find the lowest energy for the whole system. Fig. 7 represents the most stable low energy configuration for the adsorption of inhibitors on Fe (110) surface obtained through the Monte Carlo simulations.

The parameters presented in Table 7 include, the total energy, in  $\text{kJ mol}^{-1}$ , of the substrate–adsorbate configuration. The total energy is defined as the sum of the energies of the adsorbate components, the rigid adsorption energy and the deformation energy, adsorption energy reports the energy released (or required) when the relaxed adsorbate component was adsorbed on the substrate. The adsorption energy is defined as the sum of the rigid adsorption energy and the deformation energy for the adsorbate component. The rigid adsorption energy reports the energy released (or required) when the unrelaxed adsorbate component (before the geometry optimization step) was adsorbed on the substrate. The deformation energy reports the energy released when the adsorbed adsorbate component was relaxed on the substrate surface. Finally,  $(dE_{ad}/dN_i)$  reports the energy of substrate–adsorbate configurations where one of the adsorbate components has been removed[68,69].

It is by and large recognized that the essential phenomenon of corrosion inhibition of carbon steel is by adsorption. So the adsorption energy can furnish us with immediate information about the efficiency of inhibitors. The results depicted in Table 7 show that the both compounds associated with high negative values of adsorption energy resulting in the strong interactions between metal and inhibitor molecules [70]. By inspection of the Fig. 7, it could be observed that the benzodiazepine derivatives adsorb nearly to Fe (110) surface, where a chemical interactions can possibly occur through reactive sites in the molecule as interpreted in experimental and theoretical study[71].

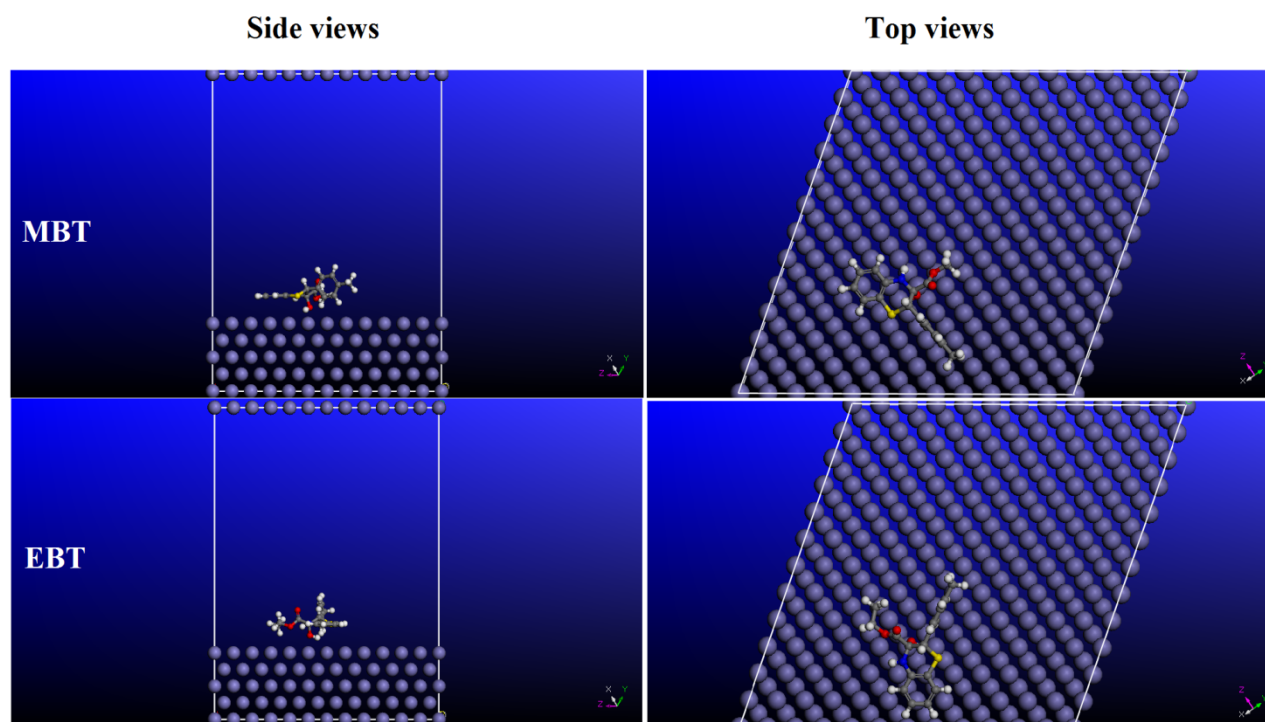


**Figure 7.** The most stable low energy configuration for the adsorption of the inhibitors on Fe (1 1 0) surface obtained through the Monte Carlo simulation.

**Table 7.** Adsorption energy calculated by the Monte Carlo simulation of inhibitors on Fe (110) surface (in kcal/mol).

System	Adsorption energy
Fe (110)/MBT	-678.34
Fe (110)/EBT	-655.43

## Conclusion

In the current paper, the corrosion inhibition of mild steel in 1.0 M HCl solutions by two benzothiazine derivatives was studied using common electrochemical techniques, quantum chemical calculations and Monte Carlo simulations. Both compounds are good corrosion inhibitors for the mild steel protection in acid solution. The inhibitory efficiency of these compounds depends on its concentration. EIS plots indicated that  $R_p$  values increase and  $C_{dl}$  values decrease with increasing inhibitor concentration. Polarization curves indicated that both compounds act as mixed type inhibitors. The adsorption of tested inhibitors on the steel surface follows Langmuir adsorption isotherm. The quantum chemical parameters are obtained and discussed in view of experimental results. Both experimental, quantum chemical and Monte Carlo simulations results showed that the inhibition efficiency of both inhibitors is affected by the heteroatoms and  $\pi$ -system presented in our compounds.

## References

1. E.H.A. Addi, L. Bazzi, M. Hilali, E.A. Zine, R. Salghi, S.E. Issami, *Can. J. Chem.* 81 (2003) 297–306.
2. R. Salghi, L. Bazzi, B. Hammouti, S. Kertit, A. Bouchart, Z. El Alami, *Ann. Chim. Sci. Matér.* 25 (2000) 593–600.
3. R. Salghi, L. Bazzi, B. Hammouti, A. Bouchart, S. Kertit, Z.A. Ait Addi, Z. El Alami, *Ann. Chim. Sci. Matér.* 25 (2000) 187–200.
4. H. Zarrok, A. Zarrouk, B. Hammouti, R. Salghi, C. Jama, F. Bentiss, *Corros. Sci.* 64 (2012) 243–252.
5. N.S. Patel, J. Hadlicka, P. Beranek, R. Salghi, H. Bouya, H.A. Ismat, B. Hammouti, *Port. Electrochimica Acta.* 32 (2014) 395–403.
6. L. Afia, R. Salghi, A. Zarrouk, H. Zarrok, E.H. Bazzi, B. Hammouti, M. Zougagh, *Trans. Indian Inst. Met.* 66 (2013) 43–49.
7. A. Bousskri, A. Anejjar, M. Messali, R. Salghi, O. Benali, Y. Karzazi, S. Jodeh, M. Zougagh, E.E. Ebenso, B. Hammouti, *J. Mol. Liq.* 211 (2015) 1000–1008.
8. L. Bammou, M. Belkhaouda, R. Salghi, O. Benali, A. Zarrouk, H. Zarrok, B. Hammouti, *J. Assoc. Arab Univ. Basic Appl. Sci.* 16 (2014) 83–90.
9. R. Salghi, L. Bazzi, M. Zaafrani, *Acta Chim. Slov.* 50 (2003) 491–504.
10. R. Salghi, M. Mihit, B. Hammouti, L. Bazzi, *J. Iran Chem Res.* 2 (2009) 157–162.
11. R.N. Singh, A. Kumar, R.K. Tiwari, P. Rawat, *Spectrochim. Acta. A. Mol. Biomol. Spectrosc.* 112 (2013) 182–190.
12. H. Jafari, I. Danaee, H. Eskandari, M. RashvandAvei, *J. Mater. Sci. Technol.* 30 (2014) 239–252.
13. L.M. Rodríguez-Valdez, W. Villamizar, M. Casales, J.G. González-Rodríguez, A. Martínez-Villafañe, L. Martínez, D. Glossman-Mitnik, *Corros. Sci.* 48 (2006) 4053–4064.
14. M. Deshmukh, S. Deshmukh, S. Jagtap, A. Mulik, *Synthesis and study of biological activity of some new 1, 4-benzothiazines*, *Ind. J. Chem.* 46B (2007) 852–859.
15. D. Armenise, G. Trapani, V. Arrivo, E. Laraspata, F. Morlacchi, *J. Heterocycl. Chem.* 37 (2000) 1611–1616.
16. D. Armenise, N. De Laurentis, A. Rosato, F. Morlacchi, *J. Heterocycl. Chem.* 43 (2006) 1371–1378.
17. M. Kumar, K. Sharma, R. Samarth, A. Kumar, *Eur. J. Med. Chem.* 45 (2010) 4467–4472.
18. R. Gupta, V. Gupta, *Heterocycl. Commun.* 16 (2010) 65–71.
19. L. Thomas, A. Gupta, V. Gupta, *J. Fluor. Chem.* 122 (2003) 207–213.
20. M. Ellouz, H. Elmsellem, N.K. Sebbar, H. Steli, K. Al Mamari, A. Nadeem, E.M. Essassi, I. Abdel-Rahaman, P. Hristov, *J. Mater. Env. Sci* 7 (7) (2016) 2482–2497.
21. I.B. Obot, D.D. Macdonald, Z.M. Gasem, *Corros. Sci.* 99 (2015) 1–30.
22. H. Lgaz, R. Salghi, M. Larouj, M. Elfaydy, S. Jodeh, Z. Rouifi, B. Lakhrissi, H. Oudda, *J. Mater. Environ. Sci.* 7 (2016) 4471–4488.
23. Materials Studio, Revision 6.0, Accelrys Inc., San Diego, USA, 2013.
24. B. Delley, *J. Chem. Phys.* 92 (1990) 508–517.
25. B. Delley, *J. Chem. Phys.* 113 (2000) 7756–7764.
26. L. Afia, R. Salghi, L. Bammou, E. Bazzi, B. Hammouti, L. Bazzi, A. Bouyanzer, *J. Saudi Chem. Soc.* 18 (2014) 19–25.
27. L. Afia, R. Salghi, A. Zarrouk, H. Zarrok, E.H. Bazzi, B. Hammouti, M. Zougagh, *Trans. Indian Inst. Met.* 66 (2013) 43–49.
28. D. Daoud, T. Douadi, S. Issaadi, S. Chafaa, *Corros. Sci.* 79 (2014) 50–58.
29. I. Ahamad, R. Prasad, M.A. Quraishi, *Corros. Sci.* 52 (2010) 933–942.

30. P. Singh, A. Singh, M.A. Quraishi, J. Taiwan Inst. Chem. Eng. (n.d.).
31. N.A. Odewunmi, S.A. Umoren, Z.M. Gasem, J. Environ. Chem. Eng. 3 (2015) 286–296.
32. N.O. Eddy, H. Momoh-Yahaya, E.E. Oguzie, J. Adv. Res. 6 (2015) 203–217.
33. M. Yadav, R. Sinha, S. Kumar, T. Sarkar, RSC Adv. 5 (2015) 70832–70848.
34. D.K. Yadav, B. Maiti, M. Quraishi, Corros. Sci. 52 (2010) 3586–3598.
35. C. Verma, M.A. Quraishi, L.O. Olasunkanmi, E.E. Ebenso, RSC Adv. 5 (2015) 85417–85430.
36. M.A. Amin, M. Ahmed, H. Arida, T. Arslan, M. Saracoglu, F. Kandemirli, Corros. Sci. 53 (2011) 540–548.
37. M.A. Amin, S.A. El-Rehim, E. El-Sherbini, R.S. Bayoumi, Int J Electrochem Sci. 3 (2008) 199–215.
38. C. Verma, E.E. Ebenso, I. Bahadur, I.B. Obot, M.A. Quraishi, J. Mol. Liq. 212 (2015) 209–218.
39. G. Moretti, F. Guidi, F. Fabris, Corros. Sci. 76 (2013) 206–218.
40. S. Kharchouf, L. Majidi, M. Bouklah, B. Hammouti, A. Bouyanzer, A. Aouniti, Arab. J. Chem. 7 (2014) 680–686.
41. R. Solmaz, Corros. Sci. 52 (2010) 3321–3330.
42. N. Labjar, F. Bentiss, M. Lebrini, C. Jama, Int. J. Corros. 2011 (2011).
43. R. Solmaz, Corros. Sci. 81 (2014) 75–84.
44. R. Solmaz, E. Altunbaş Şahin, A. Döner, G. Kardaş, Corros. Sci. 53 (2011) 3231–3240.
45. R. Yıldız, T. Doğan, İ. Dehri, Corros. Sci. 85 (2014) 215–221.
46. C. Verma, E.E. Ebenso, I. Bahadur, I.B. Obot, M.A. Quraishi, J. Mol. Liq. 212 (2015) 209–218.
47. C. Verma, M.A. Quraishi, A. Singh, J. Mol. Liq. 212 (2015) 804–812.
48. D.K. Singh, S. Kumar, G. Udayabhanu, R.P. John, J. Mol. Liq. 216 (2016) 738–746.
49. T. Laabaissi, H. Lgaz, H. Oudda, F. Benhiba, H. Zarrok, A. Zarrouk, A. El Midaoui, B. Lakhrissi, R. Tourir, J. Mater. Environ. Sci. 8 (2017) 1054–1067.
50. Y. El Aoufir, J. Sebhaoui, H. Lgaz, Y. El Bakri, A. Zarrouk, F. Bentiss, A. Guenbour, E.M. Essassi, H. Oudda, J. Mater. Environ. Sci. 8 (2017) 2161–2173.
51. H. Lgaz, R. Salghi, S. Jodeh, B. Hammouti, J. Mol. Liq. 225 (2017) 271–280.
52. M. Messali, H. Lgaz, R. Dassanayake, R. Salghi, S. Jodeh, N. Abidi, O. Hamed, J. Mol. Struct. 1145 (2017) 43–54.
53. H. Lgaz, K. Subrahmanya Bhat, R. Salghi, Shubhalaxmi, S. Jodeh, M. Algarra, B. Hammouti, I.H. Ali, A. Essamri, J. Mol. Liq. 238 (2017) 71–83.
54. Y. El Aoufir, Y. El Bakri, H. Lgaz, A. Zarrouk, R. Salghi, I. Warad, Y. Ramli, A. Guenbour, E.M. Essassi, H. Oudda, J. Mater. Environ. Sci. 8 (2017) 3290–3302.
55. M.J. Dewar, W. Thiel, J. Am. Chem. Soc. 99 (1977) 4899–4907.
56. R.G. Pearson, Inorg. Chem. 27 (1988) 734–740.
57. V. Sastri, J. Corrosion. 53 (1997) 617–622.
58. I. Lukovits, E. Kalman, F. Zucchi, Corrosion. 57 (2001) 3–8.
59. M. Lebrini, F. Bentiss, N.-E. Chihib, C. Jama, J.P. Hornez, M. Lagrenée, Corros. Sci. 50 (2008) 2914–2918.
60. Z. Cao, Y. Tang, H. Cang, J. Xu, G. Lu, W. Jing, Corros. Sci. 83 (2014) 292–298.
61. A. Kokalj, Chem. Phys. 393 (2012) 1–12.
62. N. Kovačević, A. Kokalj, Corros. Sci. 53 (2011) 909–921.
63. A. Kokalj, Electrochimica Acta. 56 (2010) 745–755.
64. J. Saranya, P. Sounthari, K. Parameswari, S. Chitra, Measurement. 77 (2016) 175–186.
65. S.K. Saha, P. Ghosh, A. Hens, N.C. Murmu, P. Banerjee, Phys. E Low-Dimens. Syst. Nanostructures. 66 (2015) 332–341.
66. Y. Sasikumar, A.S. Adekunle, L.O. Olasunkanmi, I. Bahadur, R. Baskar, M.M. Kabanda, I.B. Obot, E.E. Ebenso, J. Mol. Liq. 211 (2015) 105–118.
67. N. Karakus, K. Sayin, J. Taiwan Inst. Chem. Eng. 48 (2015) 95–102.
68. Y. El Aoufir, H. Lgaz, K. Toumiat, R. Salghi, S. Jodeh, M. Zougagh, A. Guenbour, H. Oudda, Res. J. Pharm. Biol. Chem. Sci. 7 (2016) 1200–1208.
69. L. Afia, O. Hamed, M. Larouj, H. Lgaz, S. Jodeh, R. Salghi, 70.9 (2017): 2319–2333.
70. K. Khaled, M.A. Amin, Corros. Sci. 51 (2009) 2098–2106.
71. Z. Zhang, N. Tian, X. Huang, W. Shang, L. Wu, RSC Adv. 6 (2016) 22250–22268.

(2018) ; <http://www.jmaterenvirosci.com>